Materials Advances

REVIEW

View Article Online
View Journal | View Issue

Cite this: *Mater. Adv.*, 2025, 6, 3416

Unveiling the synergy between plasma and metal–organic frameworks for next-generation materials: an overview

Amin Moghaddasfar, [a] Ghodsi Mohammadi Ziarani, [b] Rafael Luque *[cd] and Alireza Badiei *[a]

Received 22nd February 2025,
Accepted 1st May 2025

DOI: 10.1039/d5ma00171d

rsc.li/materials-advances

Plasma is a cutting-edge technology that can revolutionize synthesis methods and uniquely develop next-generation materials compared to conventional methods. The combination of plasma technology and chemical processes can open new avenues in industrial and environmental applications. This contribution aims to delve into the advantages of the plasma-assisted technique in the synthesis of metal–organic frameworks, including its effect on reaction time, morphology, porosity, stability, and crystallinity. Synergistic effects between plasma and metal–organic frameworks in various application areas, such as catalysis, chemical conversion, water treatment, and pollution remediation over conventional methods are discussed.

1. Introduction

Metal–organic frameworks (MOFs) have gained large attention from researchers and scientists due to their high porosity and activity.[1,2] MOFs comprise a new category of solid porous crystalline materials that assemble into multidimensional periodic lattices with organic linkers, coordination polymers, and inorganic nodes (clusters or cations).[3–5] Due to their particular features of porosity, large specific surface area, and crystalline nature, MOFs have emerged as promising materials for various applications such as catalytic reactions,[6] CO_2 adsorption,[7] chemical conversions,[8,9] water/wastewater treatment[10,11] and electrochemical reactions.[12,13] According to research, a wide range of synthesis methods have been used to synthesize MOFs including solvothermal,[14] hydrothermal,[15,16] microwave synthesis,[17] sonochemical,[18,19] and plasma-assisted methods.[20] MOFs can be synthesized with high crystallinity *via* solvothermal and hydrothermal methods. In microwave synthesis, MOFs can be synthesized within a shorter time. Sonochemical methods can lead to a significant decrease in crystallization time and homogeneous nucleation compared to other conventional synthesis methods. However, conventional synthesis methods typically demand high energy consumption, complicated processes and long reaction times.[21–26] The two significant limitations of MOFs synthesis by conventional methods are the time consumption and water instability. The time consumption synthesis of MOFs can take more than 1 h (certain types of MOFs can take up to 24 h) to synthesize. In addition, controlling the synthesis conditions is very difficult on a large scale.[27,28] The instability of MOFs in water can limit the utilization of these materials in different applications.[29,30] Recently, plasma-assisted synthesis has been widely employed for MOFs synthesis due to its numerous benefits,[31] successfully overcoming most shortcomings related to conventional methods.

The word "plasma," which was first introduced by William Crookes, is known as the fourth state of matter and is approximately composed of positive ions, negative electrons, radicals, molecules, and highly excited atomic species.[32,33] Through the ionization of neutral gas with sufficient energy, plasma is generated.[34] The gas ionization process occurs through the collision of electrons with gas atoms or molecules, and by absorbing energy from the electrons, it can be ionized. Depending on the type of gas and plasma source, the reactivity of the secondary species (*e.g.*, active radicals and ions) changes.[35–37] Generally, plasma is categorized into low-temperature and high-temperature plasma (Fig. 1). High-temperature plasma completely ionizes gas, while low-temperature plasma partially ionizes gas.[38,39] Low-temperature plasma is generally divided into two groups: non-thermal plasma (NTP) or cold plasma and thermal plasma. On the one hand, cold plasma is characterized by a low temperature of gas (T_g) and a high temperature of electron (T_e), and the system is in a non-equilibrium state. Furthermore, it is found to be a facile, selective effect, fast, and

[a] *Department of Chemistry, University of Tehran, Iran. E-mail: abadiei@ut.ac.ir*
[b] *Department of Organic Chemistry, Faculty of Chemistry, Alzahra University, Iran*
[c] *Peoples Friendship University of Russia (RUDN University), 6 Miklukho Maklaya Str., 117198, Moscow, Russian Federation*
[d] *Universidad ECOTEC, Km. 13.5 Samborondón, Samborondón, EC092302, Ecuador. E-mail: rluque@ecotec.edu.ec*

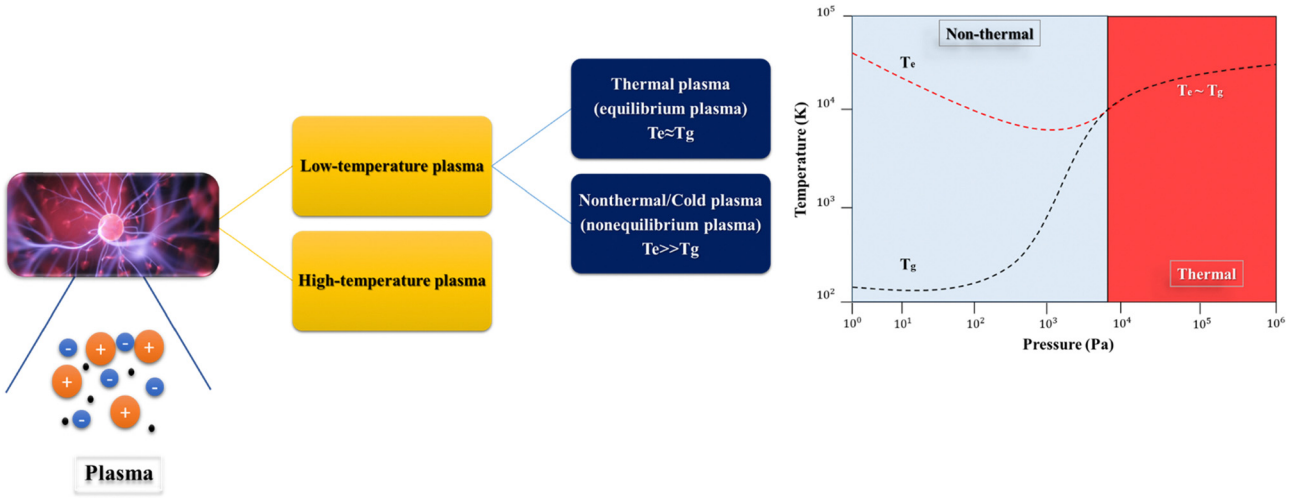

Fig. 1 Schematic of the plasma classification. Reproduced from ref. 51 with permission from RSC, copyright 2024.

environmentally friendly method for synthesizing materials.[40–43] On the other hand, thermal plasma exhibits the same gas and electron temperature and thermal equilibrium state. Thermal plasma has been mainly used in cleaning technology, coating techniques, destruction of waste materials, and extractive metallurgy.[44–46] Cold-plasma has been widely used in plasma-assisted synthesis due to its prone to reactions in room temperature conditions and low energy consumption. NTP operates at near room temperature and also at atmospheric pressure as pulsed corona,[47] dielectric barrier discharge (DBD),[48] corona discharge,[49] and radiofrequency plasma.[50]

As mentioned above, plasma can serve as an effective alternative method for synthesizing materials, specifically MOFs. In recent years, plasma-assisted synthesis of MOFs has been increasingly reported, and synergistic effects between MOFs as catalysts and plasma have been investigated. This review first aims to discuss the advances in MOF synthesis by plasma and highlight the effect of plasma on the synthesis time, morphology, topology, activity, stability, and porosity of MOFs. The second part investigates the synergistic effect between MOF and plasma in catalytic, electrocatalytic, conversion, water treatment, and volatile organic compounds removal applications.

2. Plasma-assisted synthesis of MOFs

The plasma-assisted method is a state-of-the-art technology that has been used for material synthesis and modifications. This section focuses on the effects of plasma-assisted methods specifically concerning the production of a wide variety of MOFs. The latest method and effects of plasma on MOFs are presented.

2.1. Effects of plasma

Plasma is generated by applying high energy such as electrical energy in the gaseous, which can separate gas into the ionic species and free active radicals. These secondary active species can prepare a suitable condition for the synthesis of materials.

The stability limitation of MOFs in the aqueous media has been ultimate to be a significant problem for these substances. Accordingly, NTP/cold plasma synthesis has been suggested to solve the problem. Karimzadeh *et al.*[52] reported a one-pot cold plasma Co-MOF–rGO nanocomposite synthesis under ambient conditions (Fig. 2). In this study, the Co-MOF–rGO nanocomposite was prepared by a DBD cold plasma device (300 mm in length with a 14.5 mm inner diameter, powered by an alternating current (AC) power supply of 130 W at 14 kHz). The obtained results showed that the plasma synthesis method could produce a more porous 3D nanostructure and modify the morphological structure. Furthermore, the layered regularity of Co-MOF became better when the voltage of the plasma was increased.

Kanno and co-workers[53] reported the synthesis of MOF (HKUST-1) containing Cu(I) in liquid-contacting gas-phase DBD plasma. The plasma-assisted method was compared with conventional heating (CH) and room temperature (RT) synthesis methods. This study included *in situ* treatment by plasma through the synthesis, which was also MOF activated. The results showed that the plasma-based synthesis of HKUST-1 (PL-HKUST-1) had phase-pure formation compared with conventional methods. HKUST-1 with high water stability and higher Cu(I) content could be obtained in the plasma-assisted method compared with conventional synthesis methods. To evaluate the resistance of HKUST-1 in water, it was immersed in water at ambient conditions for 12 h. After plunging, the morphology of RT-HKUST-1 and CH-HKUST-1 were thread-like, suggesting HKUST-1 decomposition. On the other hand, the morphology and size of PL-HKUST-1 remained the same after water immersion. PL-HKUST-1 was more water resistant than other conventional methods and could retain a high surface area after immersion in water. Several factors were considered for the PL-HKUST-1 water resistivity compared to other methods. First, the higher Cu(I) content of PL-HKUST-1. Second, HKUST-1 was treated with oxygen (O_2) plasma, which inhibited water molecules adsorption. The adsorption of O_2 on the state of the open metal

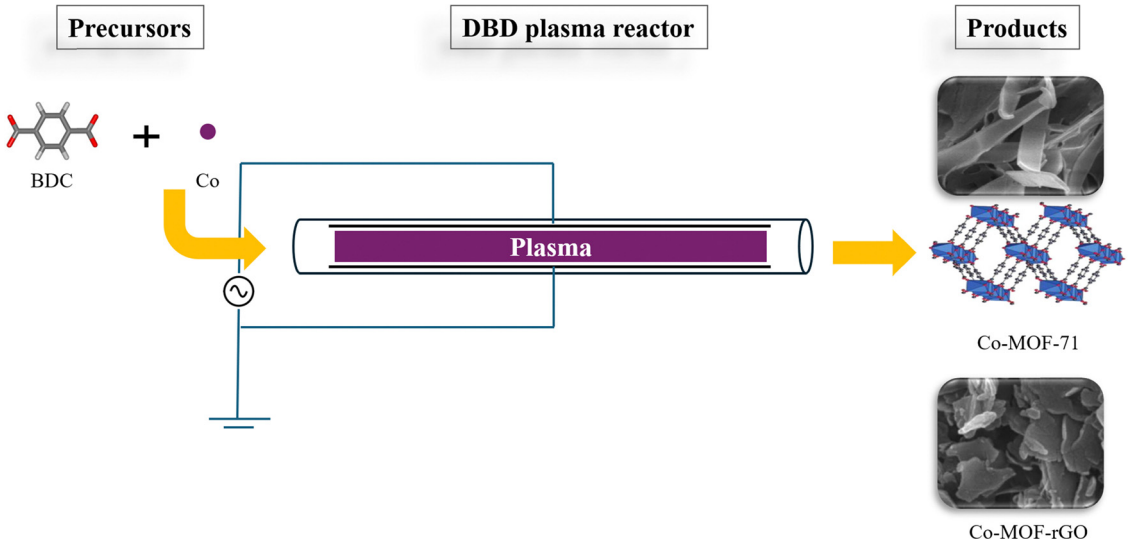

Fig. 2 MOF composites synthesis process schematic by DBD plasma reactor. Reproduced from ref. 52 with permission from Nature Portfolio, copyright 2023.

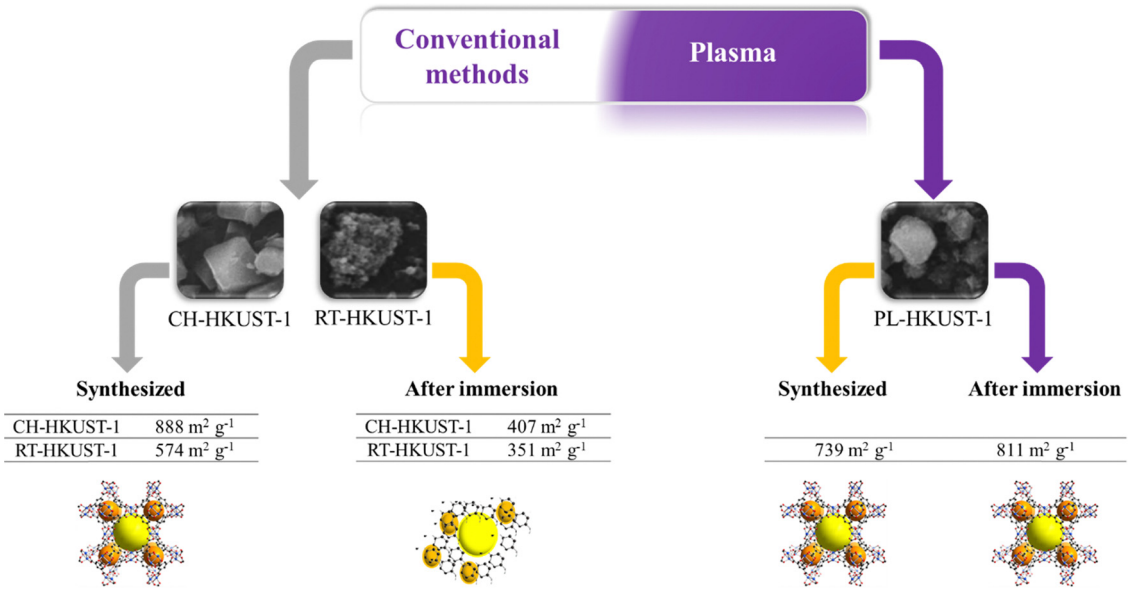

Fig. 3 Comparison of water resistance of different synthesis techniques before and after immersion in water (conventional heating method (CH-HKUST-1), room temperature (RT-HKUST-1), and plasma-assisted method (PL-HKUST-1)). Reproduced from ref. 53 with permission from RSC, copyright 2021.

site (OMS) through plasma treatment inhibited the water adsorption in the HKUST-1 structure. Another factor was the possibility of adsorption of some radicals such as O, OH, and CH on the OMS, which resulted in high water resistance of PL-HKUST-1, exhibiting good stability against degradation in water (Fig. 3).

Kan *et al.*[54] have disclosed a solution-phase synthesis using plasma to prevent defect formation in pure CPO-8-BPY membranes. In this work, CPO-8-BPY was prepared by DBD plasma (operated at 9.28 kV and 24.66 kHz). The results demonstrated that the plasma-assisted method simplified the deprotonation in the H_2aip linker, resulting in a smaller particle size and more uniform CPO-8-BPY. The XRD results indicated no significant difference between CPO-8-BPY synthesized in present and absent plasma environments. Additionally, SEM analysis revealed that the particle size distribution of as-prepared MOF with DBD plasma was narrower than that of MOF prepared without the plasma method. Karpov *et al.*[55] reported the use of low-pressure arc discharge plasma to synthesize nanopowder MOF structures based on Cu, with TEM illustrating that nanopowders were almost spherical particles and highly agglomerated with a mean size distribution of 13nm. Therefore, the high surface energy of the particles was understood. Sadakiyo *et al.*[56] employed the arc plasma deposition (APD) method to synthesize MOF composites loaded with metal nanoparticles (NPs). In this study, a wide range

of M/MOFs such as MIL-101, ZIF-8, UiO-66-NH_2, and Zn-MOF-7 as a support for various transition metal NPs such as Ru, Pd, and Pt were prepared by APD. It was mentioned that the deposited metal atoms had a similar size approximately 2 nm on the crystals of MOFs. Li *et al.*[57] have utilized the plasma-assisted method to synthesize Ce-MIL-88B(Fe) with electron-rich coordinated unsaturated metal sites (CUSs). Polyethylene terephthalate waste was used to synthesize Ce-doped MIL-88B(Fe) in the DBD plasma reactor. It was mentioned that introducing Ce substitution in Fe-MOFs altered the structure and created structural defects. The addition of Ce regulated the ratio of Fe ions and led to the formation of electron-rich CUSs. Tao *et al.*[58] have investigated Fe-based MOFs (Fe-MOFs). The Fe-MOFs were successfully synthesized utilizing the DBD plasma reactor, and the different molar ratios of trimesic acid (TA) per Fe were investigated. The results exhibited that the plasma-assisted synthesis of Fe-MOFs had some advantages, including high specific surface area, more iron-based active sites, stable crystal structure, and high pore size. In another paper, Tao *et al.*[59] have explored the effect of a broad range of discharge voltages (11.6 kV, 15.6 kV, 18 kV, and 20.8 kV) and discharge times (70 min up to 110 min) on Fe-based MOFs prepared by the DBD. The results confirmed that discharge voltage and time affect the size, crystallinity, and morphology of the as-synthesized iron-based metal–organic frameworks (Fig. 4). The XRD results indicated that by increasing the discharge voltage and time, broader and lower-intensity diffraction peaks of the samples could be obtained. Therefore, different particle sizes and crystallization could be obtained by increasing the discharge voltage and time, and this study mentioned that at 100 min discharge time and 18 kV discharge voltage, Fe-MOFs seemed to have a more uniform and regular structure.

Tang *et al.*[60] disclosed the preparation of bimetallic Fe/Ce-MOFs series with low-crystalline structures. Fe/Ce-MOFs were prepared using the DBD plasma method. The results indicated that low-crystalline Fe/Ce-MOFs had abundant oxygen defects and rich active sites. In this study, Fe/Ce-MOFs with variant Fe/Ce molar ratios and Ce-MOFs were prepared. The SEM analysis of the samples illustrated that the Fe/Ce-MOFs exhibited a structure resembling a flower, and the Ce-MOFs were rod-like structures. Therefore, the Ce-MOFs morphology changed remarkably with the introduction of Fe into the structure. Jiang *et al.*[61] have reported literature about tunable and facile construction of MOFs in DBD. In this work, the preparation of fine-tuned and diverse MOFs-based composites and MOFs in either ethanol or dimethylformamide (DMF) was proposed by an energy-saving, fast (up to 1 min) and green strategy based on the DBD technique. The results illustrated that the electrons and DMF$^{\bullet}$ generated by DBD could enhance the organic linkers deprotonation. Moreover, the produced protons from the deprotonation of the organic linkers were consumed by the production of either DMCA or H_2 (Fig. 5). With this proposed mechanism, the MOFs were synthesized by rapid kinetic, energy saving, green, and fast method compared to other conventional methods. In addition to all prepared MOFs, the crystals are characterized by high thermostability and high active surface area. It is noteworthy that in the liquid plasma synthesis method, the efficiency of the produced crystals, size, and morphology could be fine-tuned simply by controlling the synthesis processes, such as current (A), voltage (V), and time of reaction. Therefore, the appropriate energy for MOFs nucleation and crystal growth has often been derived from the electrical work applied by the electrons. Table 1 illustrates a comparison of synthesis time and active surface area of MOFs between the plasma-assisted method and conventional methods. With some adjustment of the conditions, (1) with higher electrical work regardless of the control of the current, voltage, and time, the crystal size was increased, or the crystallinity was improved; (2) with similar electrical work over current, voltage or time, crystallinity or crystals of similar size should be prepared; (3) with the electrical work which did not clearly reduce with the concentration of the reactant, the synthesis yield increased even when it was increased by 100 times.

Metal oxide (MO)/MOFs composites (MO@Fe/Ce-MOFs) were prepared using the DBD plasma-assisted method.[66] The results illustrated distinct nanosheet-like structures for MO@Fe/Ce-MOFs. Hou *et al.*[67] disclosed the rapid preparation of lanthanide MOFs (Eu (BTB) MOFs) in DBD liquid plasma.

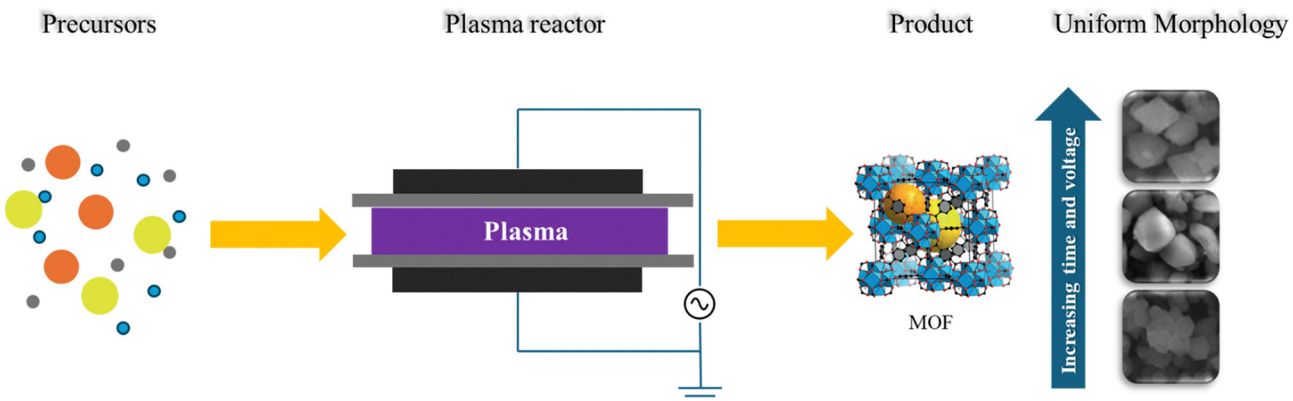

Fig. 4 Schematic preparation of MOFs by DBD plasma technique and effect of time and voltage on morphology uniformity. Reproduced from ref. 59 with permission from RSC, copyright 2019.

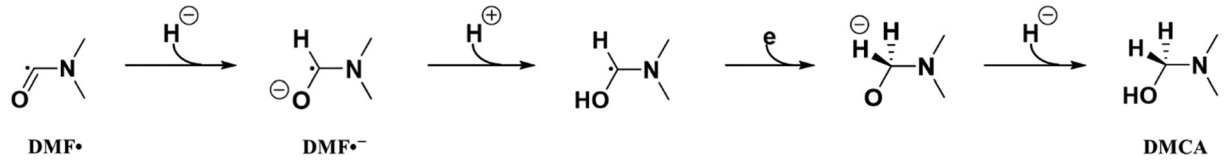

Fig. 5 Schematic of the DMCA preparation from DMF• generated by the DBD-catalyzed MOFs preparation in DBD liquid plasma. Reproduced from ref. 61 with permission from RSC, copyright 2019.

Table 1 Comparison of synthesis time and active surface area of MOFs between plasma-assisted method and conventional methods

	Conventional methods				Plasma		
MOF type	Methods	Reaction time (min)	Surface area (m^2 g^{-1})	Ref.	Reaction time (min)	Surface area (m^2 g^{-1})	Ref.
MOF-5	Solvothermal	1440	839.6	62	30	1832	61
HKUST-1	Microwave	20	1405	63	1	1680	61
ZIF-8	Sonochemical	60	1249	64	1	1400	61
UiO-66	Solvothermal	4320	1358	65	10	966	61

The proposed DBD synthesis possesses a fast preparation (within 20 min), excellent stability, and ease in simple operation and gentle conditions (ambient pressure and temperature) compared with other conventional synthesis methods. The results confirmed that the as-synthesis MOFs were endowed with great thermostability, uniform morphology, and excellent crystallinity. According to the characteristic results, Eu (BTB) MOFs appear to have a stick structure (a size between 10 and 20 μm) and a high specific surface area (446 m^2 g^{-1}). Wen and co-workers[68] have reported the plasma-assisted formation and *in situ* monitoring of three types of Ln MOFs, Tb (BDC), Eu (BTC), and Tb (BTC), ranging from variant organic ligand and metal center. In this study, the DBD synthesis method was innovatively integrated with cost-effective luminescence spectral monitoring technology to synthesize and *in situ* characterize the formation of MOFs. The SEM result indicated that the Ln-BDC synthesized by the plasma-assisted method had a 2D sheet-like framework, while Ln-BTC was a 1D ribbon-like molecular motif structure, so the split amplitude of Ln (BTC) was sharper than that of Ln (BDC).

2.2. Post-synthesis treatment

The plasma environment can facilitate the modification and treatment of materials. In this regard, Wu and colleagues[69] synthesis Fe-based MOF (MIL-100) which underwent post-synthetic treatment using glow discharge plasma (P-MIL-100) in an Ar atmosphere, generated by a high-voltage AC source, to enhance the removal of organic contaminants such as Rhodamine B and tetracycline. XRD analysis indicated that the diffraction peaks for P-MIL-100 became sharper and narrower after treatment. Furthermore, P-MIL-100 exhibited significantly greater pore size, pore volume, and specific surface area compared to the untreated MOF, resulting in improved performance in pollutant removal applications. Hou *et al.*[70] represented that Ar plasma post-synthesis treatment was applied to a titanium-based MOF (MUV-10) to manipulate the quantity of defects by varying the intensity and duration of the treatment for oxidative desulfurization purposes (Fig. 6). According to the result, this approach did not alter the crystal size or morphology. Notably, the defective MUV-10 treated for 5 minutes under 50 kV plasma demonstrated the highest concentration

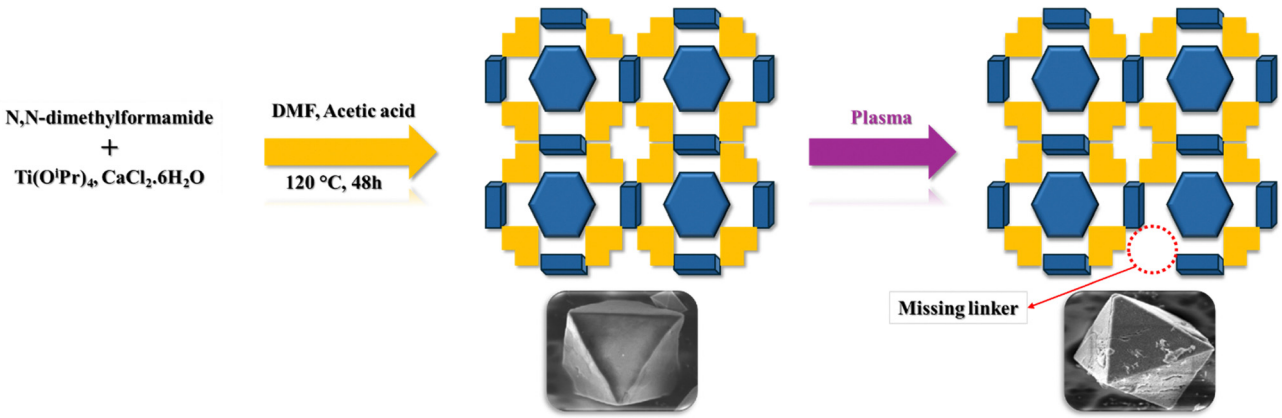

Fig. 6 Schematic of the synthesis of MUV-10 and the formation of defects during plasma treatment. Reproduced from ref. 70 with permission from Elsevier, copyright 2024.

of defects, leading to superior performance in its intended application.

The limited water and thermal stability of MOFs often pose challenges for their catalysis applications, primarily due to the role of the OMSs. The strong affinity between water molecules (H_2O) and OMSs can lead to catalyst deactivation and reduce hydrothermal stability when these materials are exposed to moisture. In this context, NTP treatment is a promising candidate that can address these limitations. Bae *et al.*[71] reported that O_2 plasma treatment is a novel method for activating and protecting the porosity of HKUST-1 when exposed to moisture. According to the results, this treatment was effective in preventing the clogging of the H_2O in the pores of the MOF (Fig. 7). The O_2 plasma acts as reactive ligands that remove coordinated H_2O and hinder the coordination of more H_2O to the unsaturated metal centers. This delay in pore-clogging occurs during exposure to moisture. A study by Xu[72] reported a practical study of a packed bed cold-plasma-activated water–gas shift reaction (WGSR) using HKUST-1. The results indicated that NTP-induced H_2O dissociation in a plasma environment generates OH that facilitate the WGSR and help prevent the water-induced HKUST-1 decomposition, thereby enhancing its stability. The O_2 plasma was effective at removing the coordinated H_2O from HKUST-1; however, the highly oxidative nature of O_2 plasma also caused damage to the MOF. In contrast, results indicated that ambient argon NTP successfully activated the as-synthesized MOF by dissociating the chemisorbed H_2O from the OMS while preserving its porous structure. An infrared vibrational spectroscopic investigation of plasma-treated MOF confirmed the removal of H_2O that were bonded to the OMSs. The NTP treatment had a minimal effect on the pore characteristics, but it improved the bulk crystallinity of the resulting plasma-treated MOF compared to the pristine sample. This treatment not only facilitates the reaction by OH but also enhances the stability and activity of plasma-treated MOF.

According to the above literature results, the plasma-assisted synthesis method is an excellent alternative to conventional synthesis methods and a promising technique for synthesizing different types of MOFs. This synthesis method is environmentally friendly and easy to prepare. In addition, with this method, the morphology, porosity, crystallinity, stability, time of synthesis, *etc.*, can be easily controlled. In comparison to conventional methods, plasma could reduce the synthesis time to less than an hour, and by adjusting the plasma voltage and gas composition, the morphology and porosity of the MOFs could be controlled. Therefore, the plasma-assisted method is a powerful method for synthesizing a broad spectrum of next-generation materials, specifically MOFs. The plasma-assisted synthesis method, similar to other conventional synthesis techniques, encounters several challenges such as reactor design, optimization of voltage and frequency, and gas composition. Addressing these challenges will require further research and theoretical studies. However, advancements in artificial intelligence and machine learning in the future could help solve these issues.

2.3. Comparison of DBD plasma-assisted MOF synthesis mechanism with hydrothermal method

The theoretical and practical aspects of the nucleation and crystal growth process of the DBD plasma-assisted MOFs synthesis method have been developed by scientists. In hydrothermal, as a conventional synthesis method, the heat increases with time, so the concentration of precursors reaches a certain level. At this point, crystals nucleate on dust particles or near the reactor walls.[73,74] However, in the DBD plasma-assisted method, a wide range of micro-discharge channels contain photons, active neutral particles, and charged particles that have been uniformly profiled on the surface of the solution film. The energy of the charged particles can be several electron volts (and the temperature in the channels is hundreds of Kelvin) due to the strong influence of the electric field. When these particles collide with the solvent, their energy is released, forming several localized superheat spots on the solution film surface. These superheat spots induced the reaction to form a precursor at atmospheric pressure and room temperature. Therefore, the precursor concentration increased with circulation, leading to nucleation growth and higher yields.[75]

Fig. 7 Proposed O_2 plasma treatment mechanism of pore activation and protection. Reproduced from ref. 71 with permission from RSC, copyright 2017.

3. Synergistic effect between plasma and MOFs

Metal–organic frameworks have remarkable properties such as high specific surface area, porosity, *etc.*, making MOFs excellent candidates for use as catalysts and solid sorbents in a wide variety of applications.[76–78] Plasma methods can create mild conditions with active species to enhance the rate of reactions.[79] Therefore, the combination of plasma and MOFs can result in a synergistic effect that improves the performance of chemical processes. In the context of MOF and plasma, synergy refers to the surplus effect of combining the MOF as a catalyst with plasma for use in specific applications. The effect of using MOF and plasma together is higher than the sum of their individual effects.[80,81] It is noteworthy that a synergistic effect does not always happen. In some cases, plasma catalytic applications may perform worse than a plasma reactor that is either empty or contains only support packing. Therefore, it is essential to identify the appropriate combinations of reaction parameters and catalyst materials.

In this section, the synergistic effect between plasma and MOFs in a wide range of fields is presented. Furthermore, the advantages and potentials of the synergistic effect in catalysis applications, chemical conversion, water treatment, and pollution remediation are evaluated.

3.1. Catalytic applications

In the past few years, plasma methods combined with MOFs have been increasingly reported. According to the research, plasma and MOFs have demonstrated an excellent synergistic effect in various applications. Xu *et al.*[82] have reported catalytic decomposition of NO_2 over a Cu/MFM-300(Al) by NTP. In this literature, a wide range of catalysts (catalysts supported by MFM-300(Al), g-Al_2O_3, and ZSM-5) and only plasma were used for NO_2 decomposition. The result revealed that the Cu/MFM-300(Al) + plasma could successfully decompose NO_2 directly into N_2O, NO, O_2, and N_2 without the utilization of other reducing agents (Fig. 8). In addition, Cu/MFM-300(Al) simultaneously exhibited high N_2 selectivity and conversion under plasma condition.

The energetic electrons produced by the plasma require appropriate energy to activate or motivate the catalysts. The electron–hole pairs (e^-/h^+) were generated by introducing energetic electrons into the catalysts. This is called pseudo-photocatalytic behavior.[83,84] Chen *et al.*[85] have studied the plasma-catalytic hybrid system. The DBD reactor with dual dielectric coaxial with a discharge length (DL) of 200 mm and discharge gap (DG) of 3.5 mm was used, which was evaluated to pseudo-photocatalyst the decomposition of ethyl acetate (EA) and nitrogen oxide (NO) simultaneously. In this work, CeO_2, $ZnGa_2O_4$, and Ce/$ZnGa_2O_4$/NH_2-UiO-66 were used as catalysts and the catalytic performances were examined. The decomposition result revealed that Ce/$ZnGa_2O_4$/NH_2-UiO-66 had the best performance compared to other catalysts. At the specific input energy (SIE) of 392 J L^{-1}, the EA and NO removal efficiencies were 96.21% and 100%, respectively. Thanks to the characteristics of the plasma-MOF catalysis system, such as the design of suitable catalysts and potential conditioning, it is a promising pathway to improve the degradation of NO_x and EA.

3.2. CO_2 and CH_4 utilization

Carbon capture, utilisation, and storage (CCUS) technology is one of most the promising technologies and plays a critical role in achieving net-zero emissions.[86–88] Carbon dioxide (CO_2) can

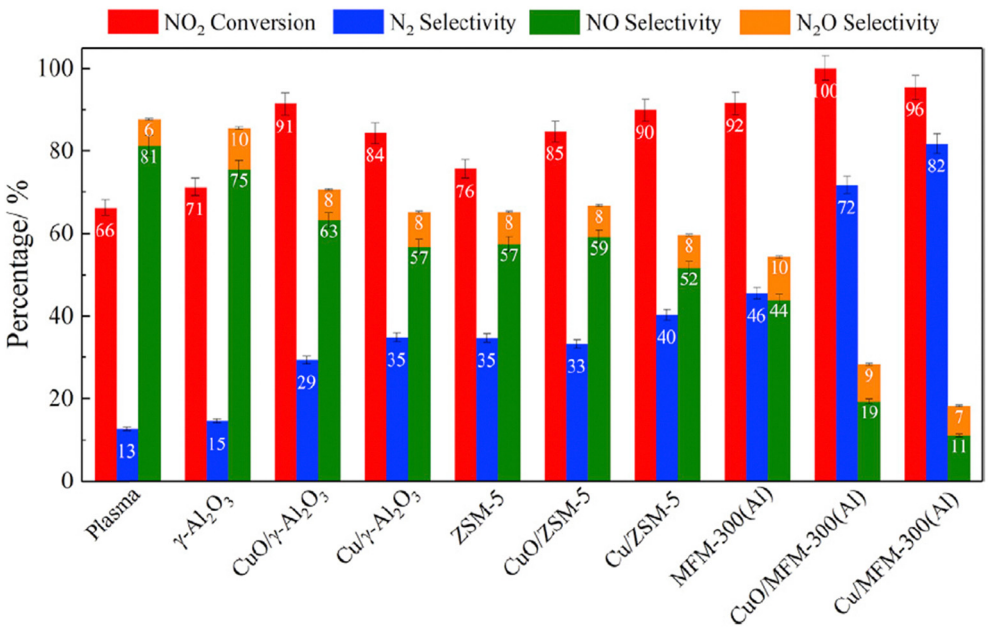

Fig. 8 Comparison of NO_2 selectivities and conversions over different catalysts and plasma only at the NTP conditions. Reproduced from ref. 82 with permission from Elsevier, copyright 2021.

be transferred into various valuable products such as specialty chemicals, fuels, hydrocarbons, *etc.*[89–91] Recently, the hydrogenation of CO_2 to ethanol has attracted scientific attention. However, the CO_2 hydrogenation has some limitations.[92,93] On the one hand, according to eqn (1), the CO_2 hydrogenation to ethanol is almost an exothermic process (lowering the process temperature is thermodynamically favorable). On the other hand, high temperatures (upper 300 °C) are needed to convert and activate CO_2 molecules effectively. These incompatible requirements posed a massive challenge to the direct preparation of ethanol (C_2H_6O) from CO_2 *via* conventional thermal catalysis. In this regard, the non-thermal plasma-catalysis technique is superior to conventional thermal systems by virtue of the low-temperature requirement, selectivity, and energy efficiency of the system.[94–98]

$$CO_2 + 4H_2 \rightarrow CH_4 + 2H_2O \quad \Delta_r H^\circ_{298\ K} = -165\ kJ\ mol^{-1} \quad (1)$$

Zou *et al.*[99] have studied the direct carbon dioxide hydrogenation to C_2H_6O under room conditions. The Cu(I)-HKUST catalyst was used in the DBD plasma reactor featuring a DL of 50 mm and DG of 3 mm. In addition, ethanol was selectively synthesized for the selective CO_2 conversion into C_2H_6O by plasma Cu(I)-HKUST catalyst (Fig. 9). The result indicated that Cu(I)-HKUST-17.5 was the best-performing catalyst, achieving 41.2% CO_2 transformation and 62.9% C_2H_6O selectivity for 2 h at 35 °C and atmospheric pressure.

Chen and co-workers[100] have explored the catalytic hydrogenation of CO_2 with 15Ni/UiO-66 under DBD plasma conditions where the gap and length discharge of the plasma reactor were 1.5 mm and 10 mm, respectively (Fig. 10). They mentioned that the DBD plasma catalysis system had approximately two-fold improved performance compared with the conventional conversion method such as thermal catalysis. Fig. 11 indicates the performance comparison of thermally activated and the DBD plasma-activated catalytic carbon dioxide hydrogenation over the 15Ni/UiO-66. According to the result, the catalyst continuous-flow DBD plasma catalysis has high catalytic activity (TOF = 1.8 ± 0.02 s^{-1}) compared with the conventional thermal method (TOF = 1.0 ± 0.06 s^{-1}). Furthermore, the stability test result confirmed that the DBD plasma catalysis was stable for approximately 20 h on stream; however, the decreasing of the catalytic performance (after 20 h TOS, CO_2 transformation decreased by about 5%) was examined under the thermal system at 380 °C (Fig. 11). Therefore, the plasma-catalytic conversion outperformed other techniques and represented the highest methane selectivity and carbon dioxide conversion at approximately 99% and 85%, respectively.

Xu *et al.*[101] have studied the plasma-catalysis carbon dioxide conversion over Ru@UiO-66. The result of DBD plasma-catalysis conversion (the DG and DL are 25 mm and 2.5 mm, with a sinusoidal peak-to-peak voltage of 19.2 kV) indicated that CH_4 selectivity and CO_2 conversion over Ru@UiO-66 reached 95.4% and 72.2%, respectively. LI *et al.*[102] have reported the plasma-assisted Co/Zr-MOF catalysis of the hydrogenation of CO_2 with an atmospheric-pressure non-thermal plasma system powered by 13 kV at 7.1 kHz (the DG was 2 mm, with inner and outer diameters of 8 mm and 10 mm, respectively). In this research, Co/Zr-MOF-M and Co/Zr-MOF-N catalysts were used for CO_2 conversion. The obtained results indicated that Co/Zr-MOF-M had a good synergy effect with atmospheric-pressure non-thermal plasma, reaching 58.9% and 94.7% for carbon dioxide conversion and methane selectivity, respectively. Xu *et al.*[103] have reported the atmospheric-pressure DBD plasma-assisted Ru/UiO-66 catalyst for hydrogenating CO_2 to CH_4. The CO_2 hydrogenation results indicated that CH_4 was selectively synthesized under the synergy effect between the plasma and Ru/Zr-MOF catalyst, and the yield of CH_4 and selectivity

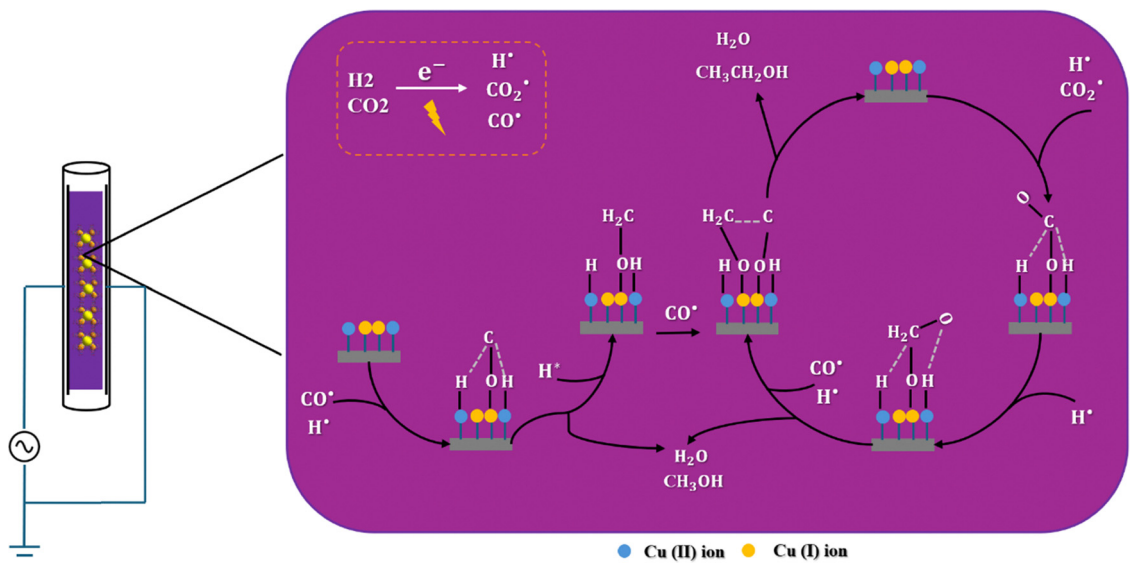

Fig. 9 The plasma-assisted ethanol synthesis mechanism on the as-synthesized catalyst. Reproduced from ref. 99 with permission from RSC, copyright 2023.

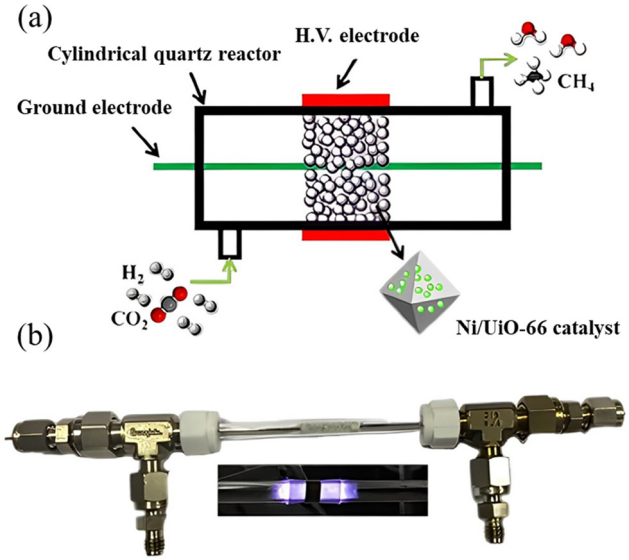

Fig. 10 (a) Schematic of DBD reactor and (b) photograph for the plasma-catalytic hydrogenation of CO_2. Reproduced from ref. 100 with permission from John Wiley and Sons, copyright 2019.

reached 39.1% and 94.6%, respectively. This study showed that the active species such as CO_2, CO, OH, H_α, CH, and C for the hydrogenation of CO_2 were confirmed by *in situ* optical emission spectra (OES) of plasma with Zr-MOF, plasma with Ru/Zr-MOF, and pure plasma. Li *et al.*[104] studied the catalysis of CO_2 hydrogenation using plasma-assisted Co/Zr-MOF-M and Co/Zr-MOF-N. The catalytic performance as-prepared MOFs was investigated by placing 0.30 g of MOFs into an atmospheric-pressure NTP quartz system, which operated at 13.0 kV and 7.1 kHz, with inner and outer diameters of 8 mm and 10 mm, respectively. The results indicated a strong synergistic effect between Co/Zr-MOF-M and NTP. At 13.0 W discharge power, with a volumetric ratio of H_2 and CO_2 of 4 : 1 and a gas flow rate of 30 mL min^{-1}, the conversion of CO_2 reached 58.9%, while the selectivity for CH_4 was an impressive 94.7%. In contrast, Co/Zr-MOF-N under the same NTP conditions achieved only a CO_2 conversion of 24.8% and a CH_4 selectivity of 9.8%.

After CO_2, CH_4 is the most prevalent greenhouse gas (GHG) emitted by human activities. Due to the stabilization of CH_4 and CO_2 concentrations in the atmosphere, their storage and conversion have been considered a promising method to reverse or stop the anthropogenic effects of CO_2 and CH_4 emissions. CH_4 has a higher global warming potential (GWP) than CO_2 because it can react with NO_x and is the cause of tropospheric ozone pollution.[105–109] For this purpose, a variety of conventional methods, such as thermal catalytic conversion, have been developed. However, CH_4 thermal catalytic conversion suffers from a wide range of challenges, such as the high temperature required for the thermal activation of CH_4, the prevention of high single-pass product yields, and the inability to achieve high selectivities and conversions simultaneously.[110–113] To overcome these challenges, cold O_2 plasma is a promising candidate for thermal catalytic conversion that is very effective for the activation of CH_4. In the NTP, high-energy electrons are accelerated by an electrical field and collide with neutral gas atoms or molecules. These collisions cause their bonds to break, producing highly active ions and free radicals. The cold plasma does not cause a considerable increase in the temperature of the bulk gas because the mass of the electrons is extremely small ($<10^{-30}$ kg). It is worth noting that while the T_e can reach 10^4–10^5 K, the T_g remains close to room temperature. The non-equilibrium properties of NTP show promise for activating thermodynamically limited reactions at room temperature, such as CH_4 oxidation and CO_2 hydrogenation.[114–118] In this regard, Gorky *et al.*[119] have studied the synergistic effect between MOF-177 and DBD plasma for methane conversion. In this study, the feasibility of desorption of the gases adsorbed on the catalyst surface employing helium plasma in the gentle pulse mode was also investigated. For the preparation of methane, oxygen and carbon dioxide were used as oxidants respectively in the presence of MOF-177. The result indicated that the maximum conversion obtained when using the $CH_4 + O_2$ system (flow ratio of $CH_4 : O_2$ of 5 : 1) was 23.5%, and the methanol selectivity was 17.65%.

According to research, the plasma-assisted non-oxidative methane coupling indicated that in the NTP system, the energy of electrons plays a critical role in the selectivity, and the hydrocarbon ionization level depends on the power input. Concretely, a low power of the electron (lower than 6 eV) favors the formation of C_2H_6 and C_3H_8, while a high energy of the electron (higher than 13 eV) favors the selective generation of C_2H_2. Therefore, in a DBD system where the power of the electrons is 5–10 eV, C_2H_6 is the dominant hydrocarbon produced.[120–122] Vakili *et al.*[123] have studied the DBD plasma-assisted catalytic dry reforming of CH_4 over UiO-67. In this literature, DBD plasma-catalysis increased the conversion of CO_2 and CH_4 by about 10% and 18%, respectively, compared to the pure plasma mode. This study confirmed that the intensity of the current pulses was increased by placing as-prepared MOF pellets in the discharge zone, indicating improved plasma generation (*i.e.*, enhanced discharge). The enhancement plasma generation by MOFs in the DBD system can be imputed to (i) the highly porous structure of MOFs, which leads to the maintenance of filamentary micro-discharges, and (ii) the high specific surface area of UiO-67, which leads to the surface discharges formation on MOFs.

The syngas (H_2/CO) production in mild reaction conditions from carbon dioxide and water presents a promising alternative to traditional chemical engineering technologies of coal-based. However, challenges arise due to the unfavorable H_2O splitting pathways, the CO_2 molecules inert nature, and the limitations of existing catalysts. These factors hinder the effective integration of high CO_2 conversion efficiency with the production of H_2/CO that has controllable H_2/CO ratios across a broad range.[124] Han *et al.*[125] have reported on an efficient and innovative DBD plasma-driven catalytic system that utilizes a high-voltage AC source with peak-to-peak voltage for the mild production of pure syngas from CO_2 and H_2O. This process

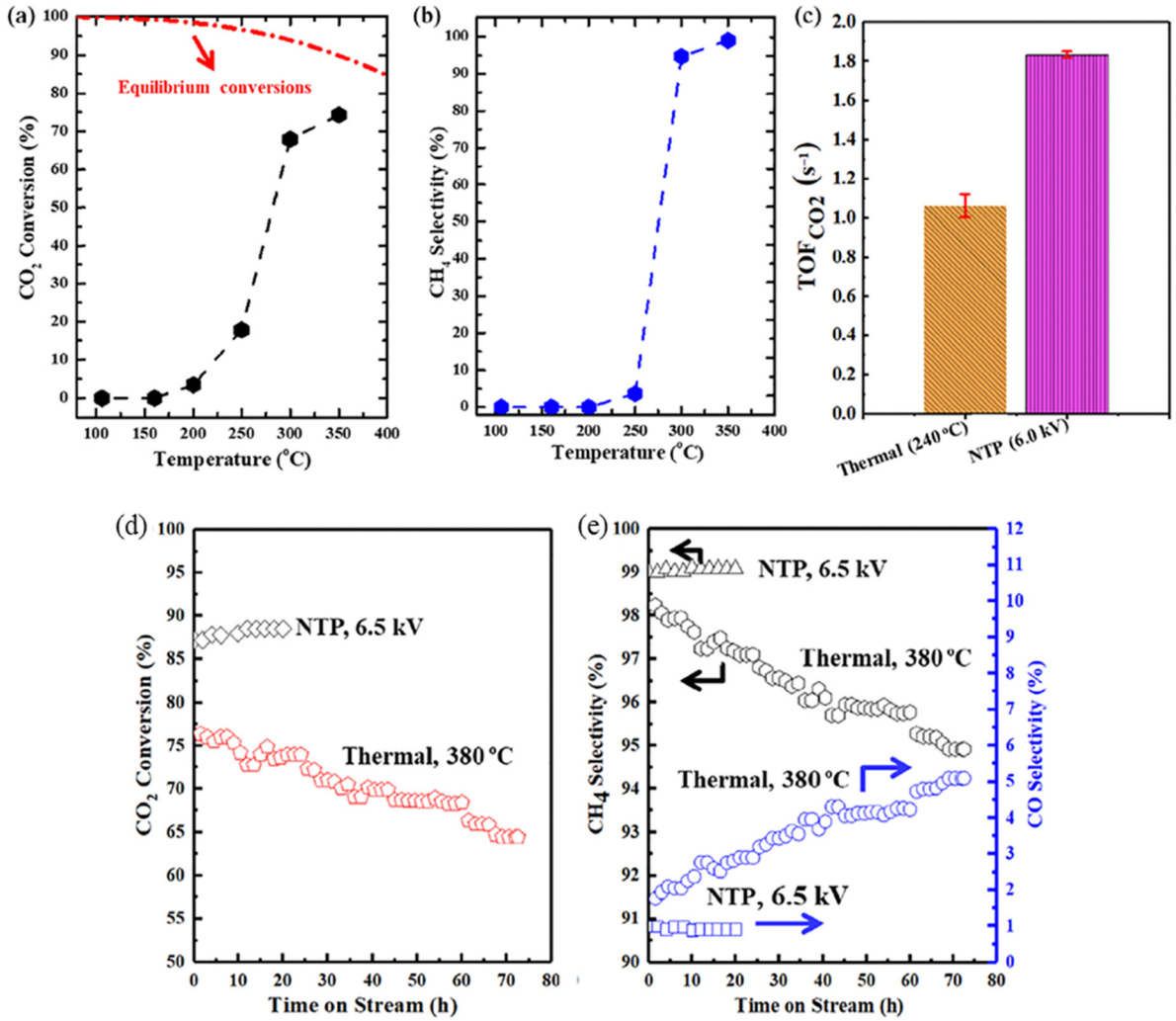

Fig. 11 Performance comparison of catalytic hydrogenation of CO_2 over the 15Ni/UiO-66 catalyst with thermal and NTP activation: (a) conversion of CO_2 and (b) selectivity of CH_4 for thermal activation, and (c) TOF amount of CO_2 conversion. The as-synthesized catalyst stability study for catalytic hydrogenation of CO_2 by thermal (380 °C) and NTP (6.5 kV) activation: (d) conversion of CO_2, (e) selectivity of CO and CH_4. Reproduced from ref. 100 with permission from John Wiley and Sons, copyright 2019.

uses porous Cu–BTC catalysts, which are rich in confined H_2O molecules. The production capacity of syngas is regulated by the *in situ* generation of ligand defects and plasma-activated intermediate species from CO_2. According to the result, the plasma not only facilitates the formation of ligand defects but also promotes structural evolution in the Cu–BTC catalyst throughout the reaction process (Fig. 12). This leads to the creation of more coordinated unsaturated metal sites, which serve as catalytically active centers with optimal coordination environments. Consequently, this catalyst system achieves a CO_2 conversion rate of 61.9% and produces pure syngas with a broad range of H_2/CO ratios from 0.05 : 1 to 4.3 : 1.

3.3. NH_3 synthesis

Ammonia (NH_3) is well known as the one of the essential chemicals in modern human society. Plasma-assisted ammonia synthesis (PAAS) offers a method for producing NH_3 by utilizing highly energetic, electronically excited N_2 and H_2 radicals at atmospheric pressure and low temperatures. This process is considered a sustainable and promising alternative to the traditional Haber–Bosch process, which relies on iron-based catalysts and operates under high temperatures (400–600 °C) and high pressures (150–350 atm). PAAS has the potential to exclusively utilize green energy sources like wind power and solar, enabling green, decentralized, and remarkable NH_3 production. However, the conventional catalysts used in PAAS face challenges, including poor stability, low efficiency, and limited cyclability.[126,127] In this regard, Liu *et al.*[128] have reported a bimetallic Co–Ni/MOF-74 catalyst for the synthesis of NH_3 in packed-bed DBD plasma (a 40 kV peak-to-peak, 40 kHz AC sinusoidal power supply was utilized, with an 80 mm DL and a 2 mm DG). In this study, a new MOF-74-supported bimetallic catalyst was developed for the synthesis of NH_3 from H_2 and N_2 in the DBD plasma at ambient conditions. A stainless steel rod served as the high-voltage electrode, connected to a mid-frequency AC sinusoidal source operating

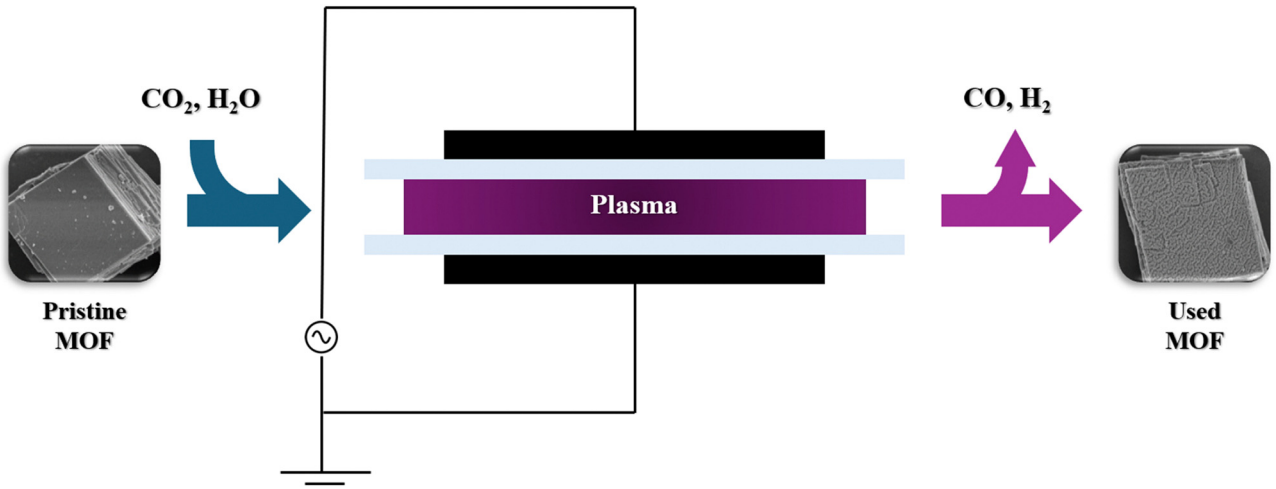

Fig. 12 Schematic of CO_2 hydrogenation *via* DBD plasma and the introduction of defects in MOFs after the plasma catalytic process. Reproduced from ref. 125 with permission from John Wiley and Sons, copyright 2024.

at a peak-to-peak voltage of 40 kV and a frequency of 40 kHz. A bed of 0.5 grams of Co–Ni/MOF-74 was positioned between the stainless steel rod and the quartz tube. The synergistic effect between Co–Ni/MOF-74 and NTP resulted in the highest NH_3 synthesis rate of 2608.70 μmol g^{-1} h^{-1} at 200 °C, with a volumetric ratio of N_2 to H_2 of 1 : 1 and a specific energy input of 33.27 kJ L^{-1}. According to the result, Co–Ni/MOF-74 catalyst + plasma indicated a higher rate of NH_3 synthesis and energy efficiency than Co–Ni/Al_2O_3 and Co–Ni/MCM-41 catalysts. Furthermore, the catalyst activity utilized for the NH_3 preparation was in the order of plasma only < Al_2O_3 < Co–Ni/Al_2O_3 < Co–Ni/MCM-41 < Co–Ni/MOF-74. Therefore, plasma + Co–Ni/MOF-74 have a good synergistic effect for NH_3 synthesis. Jing and co-workers[129] have demonstrated a one-step synthesis of Ni–Co bimetallic MOFs by the hydrothermal synthesis method for the synthesis of NH_3 in the NTP environment. The DBD plasma reactor utilized in this study includes a corundum tube that measures 480 mm in length, with inner and outer diameters of 10 mm and 15 mm, respectively. A stainless-steel rod, 5 mm in diameter and 300 mm long, serves as the high-voltage electrode and is connected to a high-voltage power supply. For the PAAS process, a catalyst powder weighing 100 mg was utilized. The Ni–Co-MOF demonstrated notably improved performance of PAAS, achieving a rate of 88.21 μmol g^{-1} min^{-1} more than a 30% increase compared to 5 wt% Ni/Al_2O_3 catalyst. Its high stability under harsh electric field conditions allows it to maintain durable performance for 36 hours and exhibit excellent cyclability over 24 cycles. The results indicate that, for the as-synthesized MOF, gas flows through the interstices of its near-spherical structure, which features a wide spectrum of interconnected pores that reduce diffusion barriers. As a result, the Ni–Co MOF demonstrates superior capabilities in gas transportation, allowing a wide range of radicals to participate in plasma atmosphere reactions within the small discharge gaps of the MOF particles. This facilitates the large number of radicals reaching the active sites, thereby enhancing the PAAS effectiveness. Furthermore, the bimetals' synergistic effect leads to further improvement in the plasma discharge performance of the as-prepared MOF and improvement in the adsorption and desorption behavior of intermediates on the catalyst surface. Song *et al.*[130] reported that Ni-MOF-74 demonstrates efficient catalytic performance for PAAS in pulsed DBD plasma. The experimental conditions included a peak pulse voltage of 16 kV, a pulse repetition frequency of 6 kHz, a rising edge of 100 ns, a falling edge of 100 ns, a pulse width of 100 ns, a total gas flow rate of 200 mL min^{-1}, and a N_2–H_2 volume ratio of 1 : 1. A total of 0.2 g of the prepared catalyst samples was packed between two layers of quartz wool inside the reactor and was uniformly dispersed in a discharge gap of 2 mm with a length of 80 mm in the DBD plasma reactor. The plasma-catalytic synthesis rate of NH_3 reached up to 41.38 mmol g^{-1} h^{-1}, with N_2 conversion rate of 1.54%. This resulted in an energy yield of 3.04 g kW h^{-1}, significantly increasing the NH_3 synthesis rate by 28.46 times, the nitrogen conversion rate by 5.7 times, and the energy yield by 5.5 times compared to plasma-only conditions. Xu *et al.*[131] published an article examining the synergistic effect of the Ni-MOF-74 catalyst and nanosecond pulsed coaxial DBD plasma on the production of PAAS. The plasma was operated at a pulse repetition frequency of 6 kHz, with a voltage of 16 kV, a rising edge of 100 ns, a falling edge of 100 ns, and a pulse width of 100 ns. In the experiment, 0.5 g of the Ni-MOF-74 was placed in the discharge area between the stainless steel rod and the quartz tube (with an outer reactor diameter of 12 mm and a wall thickness of 1 mm). Quartz wool was positioned on both sides of the discharge zone to keep the catalyst in place and prevent it from being expelled. The results demonstrated that the highest NH_3 synthesis rate achieved was 5145.16 μmol g^{-1} h^{-1}, with an energy efficiency of 1.27 g kW h^{-1}, when using the Ni-MOF-74 catalyst and N_2 to H_2 ratio of 1 : 1. This rate was 3.7 times higher than that obtained with plasma alone. A comparison of the performance of catalysts in the PAAS, as presented in Table 2.

Table 2 Comparison of the performance of catalysts in the PAAS

Method	Catalyst type	Catalyst weight (g)	N_2/H_2 molar ratio	Flow rate (mL min^{-1})	Discharge power (W)	SEI (kJ L^{-1}) energy yield	Energy yield (g kW h^{-1})	Ref.
AC DBD	Co-Ni/MOF-74	0.5	1 : 1	100	34.57	33.27	0.72	128
Pulsed DBD	Ni-MOF-74	0.2	1 : 1	200	45.61	13.68	3.04	130
Pulsed DBD	Ni-MOF-74	0.5	1 : 1	200	35.7	10.5	1.27	131
RF DBD	Ni-MOF-74	0.2	1 : 4	20	300	90	0.23	132
AC DBD	Ni/Al_2O_3	2.0	1 : 2	56	25.1	26.8	0.29	133
AC DBD	$Co–Ni/Al_2O_3$	2.0	1 : 1	200	30.81	9.24	0.83	134
AC DBD	Ru/AC	0.2	1 : 1	100	9	5.4	0.63	135
AC DBD	$La(OH)_3$	0.1	1 : 3	25	13	31.2	2.91	136

3.4. Water treatment

Drinking water is a crucial chemical in entire aspect of existence, being one of the introducing characteristics of the Earth. Approximately 97.5% of the water in oceans, only 1% of the water that is drinking water and accessible to use.[137,138] In the last decades, with the rapid development of industry, water pollution has become a significant concern for governments and scientists. In addition, sweet water scarcity is a critical challenge to the sustainable development of human civilization. Therefore, a broad range of technologies has been developed to remove water pollution.[139] The traditional approaches, such as membrane separation,[140] ozonation,[141] adsorption,[142] Fenton process,[143] photocatalytic,[144] *etc.*, have been created. However, these technologies have critical drawbacks in terms of degradation efficiency. The plasma co-catalytic system has emerged as a promising water treatment technology and has attracted the attention of scientists due to its simple operation, high efficiency, and no secondary pollutants. NTP is capable of generating highly active species, including high-energy electrons, ultraviolet (UV), H_2O_2, $^{\bullet}OH$, and O_3, which are highly reactive to react with a wide range of target hazardous pollutants.[145,146] Huang and co-workers[147] have reported enhanced degradation of norfloxacin (NOR) in water using a magnetically separable MOF-derived Co@C composite in a DBD plasma environment. According to results, the as-prepared catalyst achieved 84.7% decomposition of NOR within 25 minutes. This performance is 14.1% more effective and 10 minutes faster than that of the plasma system alone, with a synergistic factor estimated to be 1.12.

The advantages of using NTP catalytic water treatment include the absence of external oxidants, no need for temperature adjustments, and the provision of a highly efficient process. However, certain plasma technologies face significant limitations for large-scale applications due to their costs and high gas consumption. On the other hand, some MOFs can be stable in specific pH environments, limiting their maximum potential for water treatment.

3.5. Volatile organic compounds removal

The remediation of volatile organic compounds (VOCs) is crucial for controlling air pollution, as these toxic substances serve as primary precursors for $PM_{2.5}$ and regional ozone pollution. Among VOCs, toluene stands out as one of the most significant and widely used industrial chemicals. High levels of toluene emissions can lead to serious ecological harm, highlighting the importance of its removal.[148] A wide range of techniques has been employed for VOC degradation, but NTP technology is recognized as an environmentally friendly, effective, and novel approach to pollution remediation and control. NTP can initiate both chemical and physical reactions at ambient temperatures, breaking down VOCs into non-toxic byproducts such as CO_2 and H_2O.[149] In the NTP process, the utilized gas is ionized by collisions of electrons into other forms of gas atoms while releasing free-charged species such as hydroxyl radicals ($^{\bullet}OH$), singlet oxygen ($^1O_2$), superoxides ($^{\bullet}O_2^-$), and electrons (e^-). According to research, the proposed mechanism for eliminating pollutants is as follows:[150,151]

$$e^{-*} + O_2 \rightarrow {}^{\bullet}O + {}^{\bullet}O + e^- \quad (2)$$

$$e^{-*} + N_2 \rightarrow {}^{\bullet}N + {}^{\bullet}N + e^- \quad (3)$$

$$e^{-*} + H_2O \rightarrow {}^{\bullet}OH + {}^{\bullet}H + e^- \quad (4)$$

$$^{\bullet}N + O_2 \rightarrow NO + {}^{\bullet}O \quad (5)$$

$$^{\bullet}O + O_2 \rightarrow O_3 \quad (6)$$

$$O_3 + {}^{\bullet}OH \rightarrow {}^{\bullet}HO_2 + O_2 \quad (7)$$

$$^{\bullet}HO_2 + {}^{\bullet}H \rightarrow H_2O_2 \quad (8)$$

$$O_3 + H_2O \rightarrow 2{}^{\bullet}OH + O_2 \quad (9)$$

$$2{}^{\bullet}OH \rightarrow H_2O_2 \quad (10)$$

Xu and co-workers[152] studied NTP synergistic Co_xNi_y-MOF-74 for the removal of toluene. The result indicated that NTP-Co_2Ni_3-MOF outperformed NTP-Ni-MOF and NTP-Co-MOF in terms of degradation performance (showed the degradation rate of toluene 78% at 11.66 W discharge power). Rong and co-workers[153] have reported the synergistic catalytic degradation of toluene using NTP and Mn/Ce-based bimetal-organic frameworks (MCDx). According to the results, MCD_6 (Mn : Ce = 6 : 1 (molar ratio)) exhibited a good catalytic decomposition of toluene and stability, indicating toluene catalytic efficiency of 95.2%. Li and co-workers[154] explored the DBD plasma synergistic TiO_2@ZIF-8 catalyst for the simultaneous elimination of ozone and toluene (charge gap distance of 2 mm, with a peak voltage and frequency range of 4–18 kV and 6–11 kHz, respectively). The results revealed that the toluene conversion efficiency, CO_x selectivity, and O_3 decomposition efficiency were attained at 93.57%, 76.38%, and 99.22%, respectively, by

TiO_2@ZIF-8 in the NTP-catalysis system. The degradation of pollutants by NTP/cold plasma alone is a homogeneous direct reaction between pollutants and widely active free radicals and high-energy electrons excited by NTP in a gas-phase environment. However, the NTP co-catalyst system improves the gas–solid inhomogeneous reaction method on the surface of the catalyst and shows an excellent synergy effect.

As seen above, the combination of MOFs and plasma has excellent synergistic effects in various applications, increasing the reaction rate and product yield in a short time. However, the industrialization of plasma processes is challenging and requires a long path to be followed. For instance, the lack of theories of plasma processes is a major problem that should be solved first.

4. Conclusions

Plasma, as the fourth state of matter, is a promising technology for use in the synthesis, functionalization, and treatment of a broad range of materials, including organic and inorganic compounds. Beyond conventional methods, plasma offers individual advantages for the synthesis of MOFs, resulting in materials with uniform morphology, excellent crystallinity, high porosity, and high stability in water. The simultaneous use of plasma and MOF can lead to synergistic effects and advantages in various applications, thereby improving the performance of the processes, particularly in catalytic applications, chemical conversion, and pollution remediation. It is noteworthy that the synergistic effects observed with MOFs are not limited to this class of compounds but extend to a broad spectrum of materials science. Plasma has the potential to revolutionize materials synthesis, and its combination with the next generation of materials may yield synergistic effects that pave the way for innovative developments across various scientific disciplines. However, there are still many points to address and challenges to solve in the use of plasma technology and MOFs. One primary concern is that the NTP process is complex, involving a combination of disciplines such as thermodynamics, physics, chemistry, and materials science. Plasma is unable to form within the pores of catalyst supports that are usually smaller than 100 nm. This limitation arises from the insufficient free pathway for accelerating electrons in the electric field; the required free pathway is on the order of micrometers.[155] This is crucial for plasma catalysis applications because catalyst particles in these small pores will not directly interact with the plasma. Consequently, plasma active species can only reach these particles through diffusion. The extent to which plasma species can penetrate into the pores will depend on their lifetime and diffusion coefficient. Another significant challenge is the lack of *in situ* characterization techniques, which makes it difficult to analyze the process in real-time. In addition, optimizing reactor parameters and designs to create a synergistic effect between plasma and MOFs presents a crucial challenge that must be tackled. Furthermore, the limited understanding of the mechanisms behind plasma synthesis of MOFs and the scaling process represents vital areas for future research. Nonetheless, the laboratory performance of plasma-assisted MOFs has shown promise, suggesting commercial viability, but significant work remains before they can be industrialized.

Data availability

The data supporting the findings of this review article have been sourced from various journals. All relevant data and information are cited throughout the manuscript. For inquiries regarding specific datasets or materials that are not available online, please contact the corresponding author directly.

Conflicts of interest

There are no conflicts to declare.

Acknowledgements

The authors would like to express their gratitude to Prof. Leon Lefferts for his valuable comments on the manuscript. This publication has been supported by RUDN University Strategic Academic Leadership Program (R. Luque).

References

1 Y. Peng, J. Xu, J. Xu, J. Ma, Y. Bai, S. Cao, S. Zhang and H. Pang, *Adv. Colloid Interface Sci.*, 2022, **307**, 102732.
2 J. Łuczak, M. Kroczewska, M. Baluk, J. Sowik, P. Mazierski and A. Zaleska-Medynska, *Adv. Colloid Interface Sci.*, 2023, **314**, 102864.
3 R. Abazari, S. Sanati, N. Li and J. Qian, *Inorg. Chem.*, 2023, **62**, 18680–18688.
4 Y. Hu, R. Abazari, S. Sanati, M. Nadafan, C. L. Carpenter-Warren, A. M. Z. Slawin, Y. Zhou and A. M. Kirillov, *ACS Appl. Mater. Interfaces*, 2023, **15**, 37300–37311.
5 R. Abazari, S. Sanati, M. A. Bajaber, M. S. Javed, P. C. Junk, A. K. Nanjundan, J. Qian and D. P. Dubal, *Small*, 2024, **20**, 2306353.
6 C. Xu, R. Fang, R. Luque, L. Chen and Y. Li, *Coord. Chem. Rev.*, 2019, **388**, 268–292.
7 T. Ghanbari, F. Abnisa and W. M. A. Wan Daud, *Sci. Total Environ.*, 2020, **707**, 135090.
8 H.-H. Wang, L. Hou, Y.-Z. Li, C.-Y. Jiang, Y.-Y. Wang and Z. Zhu, *ACS Appl. Mater. Interfaces*, 2017, **9**, 17969–17976.
9 S. Gulati, S. Vijayan, Mansi, S. Kumar, B. Harikumar, M. Trivedi and R. S. Varma, *Coord. Chem. Rev.*, 2023, **474**, 214853.
10 F. Yang, M. Du, K. Yin, Z. Qiu, J. Zhao, C. Liu, G. Zhang, Y. Gao and H. Pang, *Small*, 2022, **18**, 2105715.
11 Y. Dai, G. Zhang, Y. Peng, Y. Li, H. Chi and H. Pang, *Adv. Colloid Interface Sci.*, 2023, **321**, 103022.
12 X. Zhang, C. Zhang, C. Yu and C. Liu, *Mater. Chem. Front.*, 2024, **8**, 1084–1100.

13 F. Parsapour, M. Moradi and A. Bahadoran, *Adv. Colloid Interface Sci.*, 2023, **313**, 102865.
14 H. Wang, Y. Dai, Y. Wang and L. Yin, *Chemosphere*, 2024, **352**, 141333.
15 W. M. Alamier, S. K. Ali, I. Y. Qudsieh, M. Imran, M. Y. A. Almashnowi, A. Ansari and S. Ahmed, *Langmuir*, 2024, **40**, 6004–6015.
16 Z. Hu, T. Kundu, Y. Wang, Y. Sun, K. Zeng and D. Zhao, *ACS Sustainable Chem. Eng.*, 2020, **8**, 17042–17053.
17 M. Wen, N. Sun, L. Jiao, S.-Q. Zang and H.-L. Jiang, *Angew. Chem., Int. Ed.*, 2024, **63**, e202318338.
18 M. A. Ashkar, S. Kutti Rani, N. Vasimalai, C.-Y. Kuo, K. Yusuf and M. Govindasamy, *Microchim. Acta*, 2024, **191**, 182.
19 C. Vaitsis, E. Kanellou, P. K. Pandis, I. Papamichael, G. Sourkouni, A. A. Zorpas and C. Argirusis, *Sustainable Chem. Pharm.*, 2022, **29**, 100786.
20 X. Xu, M. Sun, Q. Song, X. Wu, C. Chen, Q. Chen and H. Zhang, *Plasma Sci. Technol.*, 2024, **26**, 064005.
21 M. Chafiq, A. Chaouiki, J. Ryu and Y. G. Ko, *Nano Today*, 2024, **56**, 102227.
22 C. C. Obi, J. T. Nwabanne, P. K. Igbokwe, C. I. Idumah, V. U. Okpechi and H. C. Oyeoka, *J. Environ. Chem. Eng.*, 2024, **12**, 112835.
23 A. D. G. Firmino, R. F. Mendes, J. P. C. Tomé and F. A. Almeida Paz, *Metal–Organic Frameworks*, 2018, pp. 57–80, DOI: **10.1002/9783527809097.ch3**.
24 N. Stock and S. Biswas, *Chem. Rev.*, 2012, **112**, 933–969.
25 M. Safaei, M. M. Foroughi, N. Ebrahimpoor, S. Jahani, A. Omidi and M. Khatami, *TrAC, Trends Anal. Chem.*, 2019, **118**, 401–425.
26 M. Rubio-Martinez, C. Avci-Camur, A. W. Thornton, I. Imaz, D. Maspoch and M. R. Hill, *Chem. Soc. Rev.*, 2017, **46**, 3453–3480.
27 Q. He, F. Zhan, H. Wang, W. Xu, H. Wang and L. Chen, *Mater. Today Sustain.*, 2022, **17**, 100104.
28 A. Al Obeidli, H. Ben Salah, M. Al Murisi and R. Sabouni, *Int. J. Hydrogen Energy*, 2022, **47**, 2561–2593.
29 B. Liu, K. Vikrant, K.-H. Kim, V. Kumar and S. K. Kailasa, *Environ. Sci.: Nano*, 2020, **7**, 1319–1347.
30 Z. Yu, X. Cao, S. Wang, H. Cui, C. Li and G. Zhu, *Water, Air, Soil Pollut.*, 2021, **232**, 18.
31 Q. Wei, S. Xue, W. Wu, S. Liu, S. Li, C. Zhang and S. Jiang, *Chem. Rec.*, 2023, **23**, e202200263.
32 C. Ma, A. Nikiforov, D. Hegemann, N. De Geyter, R. Morent and K. Ostrikov, *Int. Mater. Rev.*, 2023, **68**, 82–119.
33 I. Adamovich, S. Agarwal, E. Ahedo, L. L. Alves, S. Baalrud, N. Babaeva, A. Bogaerts, A. Bourdon, P. J. Bruggeman, C. Canal, E. H. Choi, S. Coulombe, Z. Donkó, D. B. Graves, S. Hamaguchi, D. Hegemann, M. Hori, H. H. Kim, G. M. W. Kroesen, M. J. Kushner, A. Laricchiuta, X. Li, T. E. Magin, S. Mededovic Thagard, V. Miller, A. B. Murphy, G. S. Oehrlein, N. Puac, R. M. Sankaran, S. Samukawa, M. Shiratani, M. Šimek, N. Tarasenko, K. Terashima, E. Thomas Jr., J. Trieschmann, S. Tsikata, M. M. Turner, I. J. van der Walt, M. C. M. van de Sanden and T. von Woedtke, *J. Phys. D: Appl. Phys.*, 2022, **55**, 373001.
34 B. Ouyang, Y. Zhang, X. Xia, R. S. Rawat and H. J. Fan, *Mater. Today Nano*, 2018, **3**, 28–47.
35 S. Horikoshi, G. Brodie, K. Takaki and N. Serpone, *Agritech: Innovative Agriculture Using Microwaves and Plasmas: Thermal and Non-Thermal Processing*, Springer, 2022.
36 Y. Liu, R. Wang, C. K. Russell, P. Jia, Y. Yao, W. Huang, M. Radosz, K. A. M. Gasem, H. Adidharma and M. Fan, *Coord. Chem. Rev.*, 2022, **470**, 214691.
37 A. Fridman, *Plasma chemistry*, Cambridge university press, 2008.
38 J. Zhou, T. Wei and X. An, *Phys. Chem. Chem. Phys.*, 2023, **25**, 1538–1545.
39 L. Di, J. Zhang, X. Zhang, H. Wang, H. Li, Y. Li and D. Bu, *J. Phys. D: Appl. Phys.*, 2021, **54**, 333001.
40 K. Kyere-Yeboah, I. K. Bique and X.-C. Qiao, *Chemosphere*, 2023, **320**, 138061.
41 K. Praveen, C. Pious, S. Thomas and Y. Grohens, *Applications in Composites, Nanostructured Mateiasl and Biomedical Fields*, 2019, pp. 1–21.
42 B. Ashford and X. Tu, *Curr. Opin. Green Sustainable Chem.*, 2017, **3**, 45–49.
43 J. Zhang, X. Li, J. Zheng, M. Du, X. Wu, J. Song, C. Cheng, T. Li and W. Yang, *Energy Convers. Manage.*, 2023, **293**, 117482.
44 S. Samal, *J. Cleaner Prod.*, 2017, **142**, 3131–3150.
45 C. Puyang, J. Han and H. Guo, *Chem. Eng. J.*, 2024, **483**, 149194.
46 M. I. Boulos, P. L. Fauchais and E. Pfender, *Handbook of Thermal Plasmas*, Springer, 2023.
47 K. Song, H. Wang, Z. Jiao, G. Qu, W. Chen, G. Wang, T. Wang, Z. Zhang and F. Ling, *J. Hazard. Mater.*, 2022, **422**, 126906.
48 J. Li, C. Ma, S. Zhu, F. Yu, B. Dai and D. Yang, *Nanomaterials*, 2019, **9**, 1428.
49 H. Mahdikia, V. Brüser, M. Schiorlin and R. Brandenburg, *Plasma Chem. Plasma Process.*, 2023, **43**, 2035–2063.
50 X. Ma, J. Albertsma, D. Gabriels, R. Horst, S. Polat, C. Snoeks, F. Kapteijn, H. B. Eral, D. A. Vermaas and B. Mei, *Chem. Soc. Rev.*, 2023, **52**, 3741–3777.
51 F. Shi, J. Jiang, X. Wang, Y. Gao, C. Chen, G. Chen, N. Dudko, A. A. Nevar and D. Zhang, *Chem. Commun.*, 2024, **60**, 2700–2715.
52 Z. Karimzadeh, B. Shokri and A. Morsali, *Sci. Rep.*, 2023, **13**, 15156.
53 M. Kanno, T. Kitao, T. Ito and K. Terashima, *RSC Adv.*, 2021, **11**, 22756–22760.
54 M.-Y. Kan, Q. Lyu, Y.-H. Chu, C.-C. Hsu, K.-L. Lu, L.-C. Lin and D.-Y. Kang, *ACS Appl. Mater. Interfaces*, 2021, **13**, 41904–41915.
55 I. V. Karpov and A. V. Ushakov, *Int. J. Nanosci.*, 2020, **19**, 2050003.
56 M. Sadakiyo, S. Yoshimaru, H. Kasai, K. Kato, M. Takata and M. Yamauchi, *Chem. Commun.*, 2016, **52**, 8385–8388.
57 H. Li, M. Cheng, Z. Yang, Z. Yu, X. Tao and L. Huang, *Process Saf. Environ. Prot.*, 2024, **191**, 2599–2611.

58 X. Tao, X. Yuan, L. Huang, S. Shang and D. Xu, *RSC Adv.*, 2020, **10**, 36363–36370.
59 X. Tao, C. Sun, L. Huang, Y. Han and D. Xu, *RSC Adv.*, 2019, **9**, 6379–6386.
60 T. Tang, X. Jin, X. Tao, L. Huang and S. Shang, *J. Alloys Compd.*, 2022, **895**, 162452.
61 X. Jiang, Z. e Lin, X. Zeng, J. He, F. Xu, P. Deng, J. Jia, X. Jiang, X. Hou and Z. Long, *Chem. Commun.*, 2019, **55**, 12192–12195.
62 J. Li, S. Cheng, Q. Zhao, P. Long and J. Dong, *Int. J. Hydrogen Energy*, 2009, **34**, 1377–1382.
63 F. Zou, R. Yu, R. Li and W. Li, *ChemPhysChem*, 2013, **14**, 2825–2832.
64 Y.-R. Lee, M.-S. Jang, H.-Y. Cho, H.-J. Kwon, S. Kim and W.-S. Ahn, *Chem. Eng. J.*, 2015, **271**, 276–280.
65 Q. Zhao, W. Yuan, J. Liang and J. Li, *Int. J. Hydrogen Energy*, 2013, **38**, 13104–13109.
66 L. Huang, X. Kong, K. Chang, Z. Yu, X. Tao, T. Tang and Y. Xu, *J. Environ. Chem. Eng.*, 2023, **11**, 109836.
67 X. Hou, X. Wen, J. He and X. Hou, *Luminescence*, 2022, **37**, 2050–2058.
68 X. Wen, Y. Luo, Y. Deng, X. Zeng, Y. Tian, J. He and X. Hou, *Chem. Commun.*, 2022, **58**, 5419–5422.
69 J. Wu, Y. Gao, S. Wei, P. Chen, D. Gu, B. Fu and M. Chen, *J. Solid State Chem.*, 2021, **302**, 122350.
70 G. Hou, Y. Liu, Y. Gai, G. Han, Y. Ji, G. Hou, A. Wang, Y. Liu, P. Van Der Voort and X. Feng, *Chem. Eng. J.*, 2024, **492**, 152139.
71 J. Bae, J.-W. Jung, H. Y. Park, C.-H. Cho and J. Park, *Chem. Commun.*, 2017, **53**, 12100–12103.
72 S. Xu, S. Chansai, C. Stere, B. Inceesungvorn, A. Goguet, K. Wangkawong, S. F. R. Taylor, N. Al-Janabi, C. Hardacre, P. A. Martin and X. Fan, *Nat. Catal.*, 2019, **2**, 142–148.
73 M. Khalil, J. Yu, N. Liu and R. L. Lee, *J. Nanopart. Res.*, 2014, **16**, 2362.
74 Z. Hu, Y. Wang and D. Zhao, *Acc. Mater. Res.*, 2022, **3**, 1106–1114.
75 U. Kogelschatz, *Plasma Chem. Plasma Process.*, 2003, **23**, 1–46.
76 G. Cai, P. Yan, L. Zhang, H.-C. Zhou and H.-L. Jiang, *Chem. Rev.*, 2021, **121**, 12278–12326.
77 S. Shoaib Ahmad Shah, M. Altaf Nazir, A. Mahmood, M. Sohail, A. ur Rehman, M. Khurram Tufail, T. Najam, M. Sufyan Javed, S. M. Eldin, M. Rezaur Rahman and M. M. Rahman, *Chem. Rec.*, 2024, **24**, e202300141.
78 D. T. Sun, L. Peng, W. S. Reeder, S. M. Moosavi, D. Tiana, D. K. Britt, E. Oveisi and W. L. Queen, *ACS Cent. Sci.*, 2018, **4**, 349–356.
79 S. Liu, L. R. Winter and J. G. Chen, *ACS Catal.*, 2020, **10**, 2855–2871.
80 E. C. Neyts, K. Ostrikov, M. K. Sunkara and A. Bogaerts, *Chem. Rev.*, 2015, **115**, 13408–13446.
81 J. Kim, D. B. Go and J. C. Hicks, *Phys. Chem. Chem. Phys.*, 2017, **19**, 13010–13021.
82 S. Xu, X. Han, Y. Ma, T. D. Duong, L. Lin, E. K. Gibson, A. Sheveleva, S. Chansai, A. Walton, D.-T. Ngo, M. D. Frogley, C. C. Tang, F. Tuna, E. J. L. McInnes, C. R. A. Catlow, C. Hardacre, S. Yang and M. Schröder, *Cell Rep. Phys. Sci.*, 2021, **2**, 100349.
83 H. Wang, S. Chen, Z. Wang, Y. Zhou and Z. Wu, *Appl. Catal., B*, 2019, **254**, 339–350.
84 Z.-W. Yin, S. B. Betzler, T. Sheng, Q. Zhang, X. Peng, J. Shangguan, K. C. Bustillo, J.-T. Li, S.-G. Sun and H. Zheng, *Nano Energy*, 2019, **62**, 507–512.
85 S. Chen, W. Feng, H. Wang and Z. Wu, *Chem. Eng. J.*, 2021, **421**, 129725.
86 M. Ding, R. W. Flaig, H.-L. Jiang and O. M. Yaghi, *Chem. Soc. Rev.*, 2019, **48**, 2783–2828.
87 M. Usman, N. Iqbal, T. Noor, N. Zaman, A. Asghar, M. M. Abdelnaby, A. Galadima and A. Helal, *Chem. Rec.*, 2022, **22**, e202100230.
88 C. A. Trickett, A. Helal, B. A. Al-Maythalony, Z. H. Yamani, K. E. Cordova and O. M. Yaghi, *Nat. Rev. Mater.*, 2017, **2**, 17045.
89 O. B. Ayodele, *Appl. Catal., B*, 2022, **312**, 121381.
90 K. Y. Cohen, R. Evans, S. Dulovic and A. B. Bocarsly, *Acc. Chem. Res.*, 2022, **55**, 944–954.
91 M. D. Garba, M. Usman, S. Khan, F. Shehzad, A. Galadima, M. F. Ehsan, A. S. Ghanem and M. Humayun, *J. Environ. Chem. Eng.*, 2021, **9**, 104756.
92 V. K. Velisoju, J. L. Cerrillo, R. Ahmad, H. O. Mohamed, Y. Attada, Q. Cheng, X. Yao, L. Zheng, O. Shekhah, S. Telalovic, J. Narciso, L. Cavallo, Y. Han, M. Eddaoudi, E. V. Ramos-Fernández and P. Castaño, *Nat. Commun.*, 2024, **15**, 2045.
93 G. Zhang and Z. Xu, in *Advances in CO_2 Utilization: From Fundamentals to Applications,* ed. G. Zhang, A. Bogaerts, J. Ye and C.-j. Liu, Springer Nature, Singapore, 2024, pp. 1–36.
94 S. Saeidi, S. Najari, V. Hessel, K. Wilson, F. J. Keil, P. Concepción, S. L. Suib and A. E. Rodrigues, *Prog. Energy Combust. Sci.*, 2021, **85**, 100905.
95 J. Zhong, X. Yang, Z. Wu, B. Liang, Y. Huang and T. Zhang, *Chem. Soc. Rev.*, 2020, **49**, 1385–1413.
96 F. N. Al-Rowaili, A. Jamal, M. S. Ba Shammakh and A. Rana, *ACS Sustainable Chem. Eng.*, 2018, **6**, 15895–15914.
97 T. Len and R. Luque, *Green Chem.*, 2023, **25**, 490–521.
98 M. Tawalbeh, R. Muhammad Nauman Javed, A. Al-Othman and F. Almomani, *Energy Convers. Manage.*, 2023, **279**, 116755.
99 N. Zou, J. Chen, T. Qiu and Y. Zheng, *J. Mater. Chem. A*, 2023, **11**, 10766–10775.
100 H. Chen, Y. Mu, Y. Shao, S. Chansai, H. Xiang, Y. Jiao, C. Hardacre and X. Fan, *AIChE J.*, 2020, **66**, e16853.
101 W. Xu, M. Dong, L. Di and X. Zhang, *Nanomaterials*, 2019, 9.
102 Y. Li, J. Zhao, D. Bu, X. Zhang, T. Peng, L. Di and X. Zhang, *Plasma Sci. Technol.*, 2021, **23**, 055503.
103 W. Xu, X. Zhang, M. Dong, J. Zhao and L. Di, *Plasma Sci. Technol.*, 2019, **21**, 044004.
104 Y. Li, J. Zhao, D. Bu, X. Zhang, T. Peng, L. Di and X. Zhang, *Plasma Sci. Technol.*, 2021, **23**, 055503.

105 W.-G. Cui, G.-Y. Zhang, T.-L. Hu and X.-H. Bu, *Coord. Chem. Rev.*, 2019, **387**, 79–120.
106 K. Harrath, Z. Yao, Y.-F. Jiang, Y.-G. Wang and J. Li, *J. Phys. Chem. C*, 2024, **128**, 5579–5589.
107 Y. Ma, X. Han, S. Xu, Z. Li, W. Lu, B. An, D. Lee, S. Chansai, A. M. Sheveleva, Z. Wang, Y. Chen, J. Li, W. Li, R. Cai, I. da Silva, Y. Cheng, L. L. Daemen, F. Tuna, E. J. L. McInnes, L. Hughes, P. Manuel, A. J. Ramirez-Cuesta, S. J. Haigh, C. Hardacre, M. Schröder and S. Yang, *J. Am. Chem. Soc.*, 2023, **145**, 20792–20800.
108 F. Alahmadi, I. S. Khan, D. Poloneeva, G. Shterk, L. C. Garzon Tovar, R. Schucker, A. Bavykina and J. Gascon, *Ind. Eng. Chem. Res.*, 2022, **61**, 15195–15201.
109 T. Imyen, E. Znoutine, D. Suttipat, P. Iadrat, P. Kidkhunthod, S. Bureekaew and C. Wattanakit, *ACS Appl. Mater. Interfaces*, 2020, **12**, 23812–23821.
110 P. Schwach, X. Pan and X. Bao, *Chem. Rev.*, 2017, **117**, 8497–8520.
111 W. Taifan and J. Baltrusaitis, *Appl. Catal., B*, 2016, **198**, 525–547.
112 M. Yousefi and S. Donne, *Int. J. Hydrogen Energy*, 2022, **47**, 699–727.
113 L. He, Y. Fan, J. Bellettre, J. Yue and L. Luo, *Renewable Sustainable Energy Rev.*, 2020, **119**, 109589.
114 C. Shi, S. Wang, X. Ge, S. Deng, B. Chen and J. Shen, *J. CO2 Util.*, 2021, **46**, 101462.
115 P. Chawdhury, Y. Wang, D. Ray, S. Mathieu, N. Wang, J. Harding, F. Bin, X. Tu and C. Subrahmanyam, *Appl. Catal., B*, 2021, **284**, 119735.
116 V. Maslova, R. Nastase, G. Veryasov, N. Nesterenko, E. Fourré and C. Batiot-Dupeyrat, *Prog. Energy Combust. Sci.*, 2024, **101**, 101096.
117 C. Qi, Y. Bi, Y. Wang, H. Yu, Y. Tian, P. Zong, Q. Zhang, H. Zhang, M. Wang, T. Xing, M. Wu, X. Tu and W. Wu, *ACS Catal.*, 2024, **14**, 7707–7716.
118 X. Chen, H.-H. Kim and T. Nozaki, *Plasma Processes Polym.*, 2024, **21**, 2200207.
119 F. Gorky, A. Nambo and M. L. Carreon, *J. CO2 Util.*, 2021, **51**, 101642.
120 J. Feng, X. Sun, Z. Li, X. Hao, M. Fan, P. Ning and K. Li, *Adv. Sci.*, 2022, **9**, 2203221.
121 J. Slaets, B. Loenders and A. Bogaerts, *Fuel*, 2024, **360**, 130650.
122 R. Garcia-Villalva, M. Biset-Peiró, A. Alarcón, C. Bacariza, S. Murcia-López and J. Guilera, *Int. J. Hydrogen Energy*, 2024, **59**, 1367–1375.
123 R. Vakili, R. Gholami, C. E. Stere, S. Chansai, H. Chen, S. M. Holmes, Y. Jiao, C. Hardacre and X. Fan, *Appl. Catal., B*, 2020, **260**, 118195.
124 A. Lebouvier, S. A. Iwarere, P. d'Argenlieu, D. Ramjugernath and L. Fulcheri, *Energy Fuels*, 2013, **27**, 2712–2722.
125 Y. Han, G. Fan, Y. Guo, S. Guo, J. Ding, C. Han, Y. Gao, J. Zhang, X. Gu and L. Wu, *Angew. Chem., Int. Ed.*, 2024, **63**(29), e202406007.
126 X. Han, S. Yang and M. Schröder, *J. Am. Chem. Soc.*, 2023, **145**, 1998–2012.
127 Y. Yu, Y. Li, Y. Fang, L. Wen, B. Tu and Y. Huang, *Appl. Catal., B*, 2024, **340**, 123161.
128 Y. Liu, X. Xu, Q. Song, Z. Guo, X. Wu, C. Chen, Q. Chen and H. Zhang, *Plasma Processes Polym.*, 2024, **21**, 2300086.
129 Y. Jing, F. Gong, S. Wang, W. Wang, P. Yang, E. Fu and R. Xiao, *Fuel*, 2024, **368**, 131686.
130 Q. Song, X. Yin and H. Zhang, *Plasma Processes Polym.*, 2024, e2400173.
131 X. Xu, M. Sun, Q. Song, X. Wu, C. Chen, Q. Chen and H. Zhang, *Plasma Sci. Technol.*, 2024, **26**, 064005.
132 J. Shah, T. Wu, J. Lucero, M. A. Carreon and M. L. Carreon, *ACS Sustainable Chem. Eng.*, 2019, **7**, 377–383.
133 Y. Wang, M. Craven, X. Yu, J. Ding, P. Bryant, J. Huang and X. Tu, *ACS Catal.*, 2019, **9**, 10780–10793.
134 Y. Liu, C. W. Wang, X. F. Xu, B. W. Liu, G. M. Zhang, Z. W. Liu, Q. Chen and H. B. Zhang, *Plasma Chem. Plasma Process.*, 2022, **42**, 267–282.
135 X. Zhu, J. Liu, X. Hu, Z. Zhou, X. Li, W. Wang, R. Wu and X. Tu, *J. Energy Inst.*, 2022, **102**, 240–246.
136 K. Li, S. Chen, M. Li, L. Liu, Y. Li and F. Wang, *Int. J. Hydrogen Energy*, 2024, **59**, 1287–1296.
137 H. Zeghioud, P. Nguyen-Tri, L. Khezami, A. Amrane and A. A. Assadi, *J. Water Process Eng.*, 2020, **38**, 101664.
138 C. A. Aggelopoulos and O. Dolinski, *Chemosphere*, 2024, **347**, 140667.
139 M. Rahimpour, H. Taghvaei, S. Zafarnak, M. R. Rahimpour and S. Raeissi, *J. Environ. Chem. Eng.*, 2019, **7**, 103220.
140 M. U. Shahid, T. Najam, M. Islam, A. M. Hassan, M. A. Assiri, A. Rauf, A. u Rehman, S. S. A. Shah and M. A. Nazir, *J. Water Process Eng.*, 2024, **57**, 104676.
141 X. Kong, J. Ma, S. Garg and T. D. Waite, *Environ. Sci. Technol.*, 2024, **58**, 8988–8999.
142 M. A. Ahsan, V. Jabbari, M. T. Islam, R. S. Turley, N. Dominguez, H. Kim, E. Castro, J. A. Hernandez-Viezcas, M. L. Curry, J. Lopez, J. L. Gardea-Torresdey and J. C. Noveron, *Sci. Total Environ.*, 2019, **673**, 306–317.
143 T. Hu, L. Tang, H. Feng, J. Zhang, X. Li, Y. Zuo, Z. Lu and W. Tang, *Coord. Chem. Rev.*, 2022, **451**, 214277.
144 A. Moghaddasfar, M. Darbandi and Z.-A. Li, *J. Water Process Eng.*, 2023, **54**, 104056.
145 J. Fan, H. Wu, R. Liu, L. Meng and Y. Sun, *Environ. Sci. Pollut. Res.*, 2021, **28**, 2522–2548.
146 A. Yusuf, H. K. Amusa, J. O. Eniola, A. Giwa, O. Pikuda, A. Dindi and M. R. Bilad, *Chem. Eng. J. Adv.*, 2023, **14**, 100443.
147 L. Huang, X. Chen, B. Wan and S. Xu, *Sep. Purif. Technol.*, 2023, **306**, 122488.
148 Z. Ye, Z. Ye, A. Nikiforov, J. Chen, W. Zhou, J. Chen, G. Wang and Y. Zhang, *Chem. Eng. J.*, 2021, **407**, 126280.
149 K. H. Hama Aziz, H. Miessner, A. Mahyar, S. Mueller, D. Kalass, D. Moeller and K. M. Omer, *Sep. Purif. Technol.*, 2019, **216**, 51–57.
150 C. A. Aggelopoulos, *Chem. Eng. J.*, 2022, **428**, 131657.
151 S. Mededovic Thagard, G. R. Stratton, F. Dai, C. L. Bellona, T. M. Holsen, D. G. Bohl, E. Paek and E. R. V. Dickenson, *J. Phys. D: Appl. Phys.*, 2017, **50**, 014003.

152 Y. Xu, Z. Li, G. Qu, Y. Chen, H. Wu, P. Ning and J. Li, *Catal. Lett.*, 2024, **154**, 2891–2902.
153 X. Rong, Q. Cao, Y. Gao, T. Luan, Y. Li, Q. Man, Z. Zhang and B. Chen, *Molecules*, 2022, **27**, 7363.
154 X. Li, S. Wang, X. Zhang, D. Mei, Y. Xu, P. Yu and Y. Sun, *J. Cleaner Prod.*, 2022, **332**, 130107.
155 L. Lefferts, *Angew. Chem., Int. Ed.*, 2024, **63**(10), e202305322.